The Role of Turbomachinery Performance in the Optimization of Supercritical Carbon Dioxide Power Systems

Article *in* Journal of Turbomachinery · January 2020

DOI: 10.1115/1.4046182

CITATIONS
22

READS
745

4 authors:

Alessandro Romei
Politecnico di Milano
19 PUBLICATIONS **125** CITATIONS
SEE PROFILE

Paolo Gaetani
Politecnico di Milano
100 PUBLICATIONS **1,189** CITATIONS
SEE PROFILE

Andrea Giostri
Politecnico di Milano
20 PUBLICATIONS **627** CITATIONS
SEE PROFILE

Giacomo Persico
Politecnico di Milano
146 PUBLICATIONS **1,869** CITATIONS
SEE PROFILE

This is a preprint of the following article: Romei, A., Gaetani, P., Giostri, A., & Persico, G., *The role of turbomachinery performance in the optimization of supercritical carbon dioxide power systems*, J. Turbomach., 2020.
The published article may differ from this preprint, and is available at the following DOI: 10.1115/1.4046182

THE ROLE OF TURBOMACHINERY PERFORMANCE IN THE OPTIMIZATION OF SUPERCRITICAL CARBON DIOXIDE POWER SYSTEMS

Alessandro Romei[†], **Paolo Gaetani, Andrea Giostri, Giacomo Persico**
Energy Department, Politecnico di Milano
Via Lambruschini 4, 20156 Milan, Italy

[†]Corresponding author, alessandro.romei@polimi.it

ABSTRACT

The successful penetration of supercritical carbon dioxide (sCO_2) power systems in the energy market largely depends on the achievable turbomachinery efficiency. The present study illustrates a systematic framework where both the compressor and the turbine are designed via validated (within $\pm 2\%pts$ against experiments) mean-line tools and the subsequent impact on cycle performance estimates is quantitatively and qualitatively assessed. A significant effort is devoted to the analysis of centrifugal compressor performance operating close to the thermodynamic critical point, where sharp variations in the thermodynamic properties may make critical the compression process. The analysis is performed for different compressor sizes and pressure ratios, showing a comparatively small contribution of the compressor-intake fluid conditions to the machine efficiency, which may achieve competitive values ($82 \div 85\%$) for representative full-scale sizes. Two polynomial correlations for both the turbomachinery efficiencies are devised as a function of proper similarity parameters accounting for machine sizes and loadings. Such correlations can be easily embedded in power cycle optimizations, which are usually carried out assuming constant-turbomachinery efficiencies, thus ignoring the effects of plant size and cycle operating parameters. Efficiency correlations are finally exploited to perform several optimizations of a representative recompression sCO_2 cycle, by varying multiple cycle parameters, namely maximum and minimum temperature, pressure ratio and net power output. The results highlight that the replacement of the constant-efficiency assumption with the proposed correlations leads to more accurate performance predictions (e.g. cycle efficiency can differ by more than $4\%\,pts$), besides showing that an optimal pressure ratio exists in the range $2 \div 5$ for all the investigated configurations.

INTRODUCTION

Supercritical carbon dioxide (sCO_2) power systems represent a promising cost-effective solution for several technologies, ranging from nuclear [1] to concentrating solar power [2] and waste heat recovery [3]. In these fields of application, sCO_2 plants may prevail over conventional power systems (generally featuring steam as working fluid) thanks to the overall higher conversion efficiency, simpler plant layout and smaller turbomachinery sizes [4]. These considerations are mainly supported by techno-economic analyses of the thermodynamic cycle, which usually rely on simplified models for the main components (heat exchangers and turbomachinery).

Unfortunately, these analyses may be biased by reworking paradigms derived from conventional technologies, for which well-validated data are available. The aleatory decision to assume specific values for some parameters may determine on paper the success of a sCO_2 power system over a traditional one. An example is given by the common tendency to assume constant values for the turbomachinery efficiencies, whose choice greatly affects the overall cycle performance [5]. Besides, the arbitrary root of this choice may lead to significantly different, sometimes contradictory, results published in Open Literature (a clear example is illustrated by the survey conducted in [6]). Systematic and tailor-made rules for this specific field have yet to be devised in order to enable fair comparisons with well-established technologies. The present work aims at filling this gap with a focus on turbomachinery operating with CO_2 in the peculiar thermodynamic conditions delineated by the power cycle, providing a systematic frameworks via computational design and optimization models. The implication of turbomachinery designs and performance on the power cycle is quantitatively assessed as well.

The compressor is recognized as one of the most critical component for future sCO_2 power cycles [7]. The general expec-

This is a preprint of the following article: Romei, A., Gaetani, P., Giostri, A., & Persico, G., *The role of turbomachinery performance in the optimization of supercritical carbon dioxide power systems*, J. Turbomach., 2020.
The published article may differ from this preprint, and is available at the following DOI: 10.1115/1.4046182

tation is that the compressor may be less efficient or may exhibit more stability issues if compared to its air-breathing counterpart, resulting from operations close to the thermodynamic critical point where a sharp variation in the thermodynamic properties and local two-phase flows may possibly occur. This statement was questioned by Noall & Pash [8], who provided a preliminary analysis of a full-scale compressor featuring a comparatively high efficiency ($83 \div 85\%$). In the first part of the paper, after a proper validation of the mean-line compressor model, we support this perspective at least for compressors at design conditions, providing optimized designs and corresponding performance (in terms of efficiency) for different upstream thermodynamic conditions, pressure ratios and mass-flow rates.

Moreover, we propose a similar approach to also model the turbine, coupling an optimization strategy with a mean-line design tool. Our analysis is limited to the axial-turbine layout, because it is considered suitable for a larger range of plant capacities than the radial-inflow counterpart [4].

Then, we collect all optimized designs to build consistent polynomial correlations (separately for the compressor and for the turbine) to include realistic variations of the turbomachinery efficiencies within the framework of cycle analysis and optimization. These tailor-made correlations make it possible to properly infer about the evolution of optimal cycle parameters, such as overall pressure ratio and cycle efficiency, for different temperature levels and installed plant capacities. Finally, the potential efficiency gain achievable by multi-stage turbomachinery is investigated on a discrete number of operating conditions and the advantages in terms of cycle performance are highlighted.

1 NUMERICAL TOOLS

In this section, cycle and turbomachinery models are described and the main assumptions are clearly pointed out. In order to explore a wide range of design conditions at a reasonable computational cost, the mean-line representation is selected as simulation tool for both turbomachinery components, namely centrifugal compressors and axial turbines. The mean-line representations assumes uniform and unidirectional flow in each relevant section at midspan, hub and tip. Thanks to these simplifications, it allows determining a preliminary machine layout in terms of size, angular speed, blade heights and velocity triangles at a very low computational cost. Besides, they also provide a realistic representation of the flow path along the machine. As both codes are conceived as direct simulation tools, they need an external optimization routine for design application. Carbon dioxide properties are computed by calling the external thermodynamic library RefProp® [9], which features a multi-parameter equation of state expressed in terms of Helmholtz fundamental relation [10].

1.1 Cycle layout and model assumptions

The present analysis is carried out on a representative sCO_2 closed cycle, namely the so-called recompression cycle, whose layout is reported in Figure 1. Among the large number of cycle arrangements (see, for a review, [11]), the recompression cycle provides a high efficiency and a comparatively simple layout. The presence of an internal heat recuperation allows retrieving the residual thermal energy at the turbine outlet to preheat the compressed fluid, thus reducing both the heat input and the heat rejected to the environment. To cope with the strong variation of the fluid specific heat in the cold side, the recuperative process is split into two units operating with different mass-flow rates. In this way, it is possible to optimize the temperature profiles between hot and cold sides by acting on the thermal capacity of the cold side, so that the entropy generated by finite-temperature differences in the heat-transfer process is reduced. In this work, heat exchangers, both the primary heat exchanger and recuperators (hereinafter, LTR: low-temperature recuperator, HTR: high-temperature recuperator), are simulated with a one-dimensional approach, splitting the overall heat-transfer problem in several sub-problems whereby the fluid properties are assumed constant. A finite pinch-point temperature difference ΔT_{pp} is provided for each heat exchanger, to avoid the occurrence of negative pinch-point temperature difference when the split factor, $SF = \dot{m}_{LTR}/\dot{m}$, i.e. the ratio between the mass flow in the LTR and the overall mass flow, is varied. A dedicated routine checks where the pinch-point occurs within LTR, as the cooling process is strongly non linear due to the significant variation of CO_2 specific heat in the range of interest. Based on previous works [12], a $10\,^{\circ}C$ is imposed as a pinch-point temperature difference in the heat exchangers and a relative pressure drop $\Delta p/p_{in} = 2\%$ is considered for all heat exchangers as well. The heat input is provided by a hot source at constant temperature. Electric (both for generator and motors) and mechanical efficiencies are set at the constant value of 97% [12]. Turbomachinery are imple-

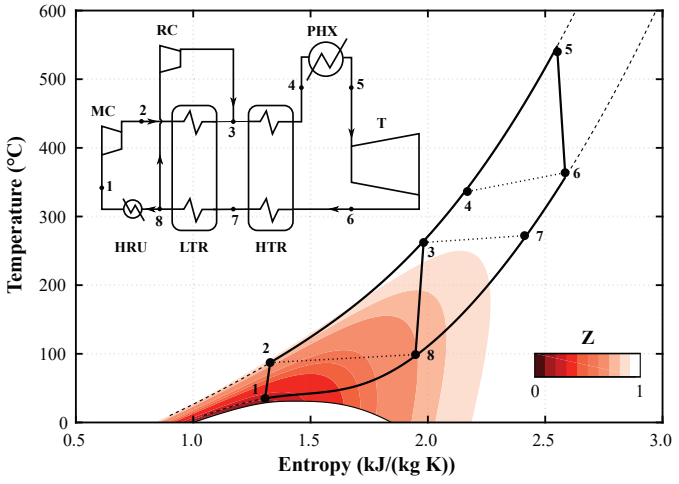

FIGURE 1: Recompression sCO_2 cycle layout and corresponding thermodynamic transformations on T–s plane. MC: Main compressor; RC: Recompressor; PHX: Primary Heat Exchanger; T: Turbine; HTR: High-Temperature Recuperator; LTR: Low-Temperature Recuperator; HRU: Heat Rejection Unit. A map of the compressibility factor $Z = Pv/RT$ is superposed.

This is a preprint of the following article: Romei, A., Gaetani, P., Giostri, A., & Persico, G., *The role of turbomachinery performance in the optimization of supercritical carbon dioxide power systems*, J. Turbomach., 2020.
The published article may differ from this preprint, and is available at the following DOI: 10.1115/1.4046182

mented either at constant isentropic efficiency or with dedicated efficiency correlations, detailed in Section 3. For each cycle, maximum and minimum pressures, along with the split factor, are varied to obtain the highest electrical efficiency, defined as $\eta_{el} = \dot{W}_{el}/\dot{Q}_{in}$, where $\dot{W}_{el}$ is the electrical power and $\dot{Q}_{in}$ is the thermal power input. To this end, a hybrid optimization routine is used, combining a genetic-based algorithm to initialize a gradient-based method. Figure 1 also reports the typical transformations on temperature–specific entropy (T–s) thermodynamic plane, fixing the cycle minimum temperature $T_{min} = 35\,°\text{C}$ and the hot-source temperature $T_{max} = 550\,°\text{C}$ and assuming constant efficiencies for the turbomachinery ($\eta_c = 0.86$ for the compressors and $\eta_t = 0.90$ for the turbine).

1.2 Mean-line tool for centrifugal compressors

The mean-line code for the design of single-stage centrifugal compressor operating with sCO_2 is based on several loss models, formulated as enthalpy variations, which account for the sources of entropy generation usually occurring in centrifugal compressors. The calculations are run by assigning the compressor geometry along with upstream total quantities and mass-flow rate. The impeller loss model is rooted in the pioneer work of Oh *et al.* [13], which was validated for sCO_2 compressor [14, 15, 16] against experimental results [7]. Five sources of losses (causing a decrease in the total-pressure rise), namely incidence, blade-loading, tip clearance, mixing and skin-friction losses, were formulated to derive the impeller efficiency. Moreover, three external losses (only contributing to an increase of the machine total enthalpy) were also considered, i.e. recirculation, disc-friction and leakage losses. The present design tool recovers the full set of losses, whose analytical expressions are reported in Table 1 for the reader's convenience. The deviation angle at the impeller outlet is estimated with the slip factor formulation provided by Wiesner [17]. Whenever splitter blades are introduced, the effective number of blades is assumed as $N_{eff} = N_{bl} + 0.75N_{spl}$, where N_{bl} represents the number of full blades and N_{spl} is the number of splitter blades.

In an effort of improving the predictive capabilities, realistic losses for the diffuser and volute, as well as their preliminary sizing, are also implemented. Two kind of losses are considered for the vaned diffuser, namely incidence and skin-friction losses, recalling the formulations available for the impeller. The skin-friction loss occurring in the vaned diffuser includes an additional factor δ_{BL}, accounting for the development of boundary layer in the impeller channel [18]. A constant skin-friction coefficient, $c_f = 0.006$, is considered in the computation of skin-friction losses for both the impeller and the vaned diffuser. This value was suggested for air-breathing compressors [19], whose operations are characterized by significantly lower Reynolds numbers with respect to the typical values found in sCO_2 compressors [20]. Besides, a dedicated analysis of the skin-friction coefficient was performed by Ameli *et al.* [15], showing that $c_f = 0.006$ is reasonably acceptable for sCO_2 centrifugal compressors. Finally, the radial component of the velocity at the diffuser outlet is dissipated to account for the volute loss. A skin-friction loss for the volute might be formulated as well, however the kinetic energy involved in this component is rather low, so that this source of loss is not expected to significantly affect the compressor performance.

The mean-line code is validated against experimental data provided by Sandia Laboratories [7] at three different rotational speeds, namely 45000 RPM, 50000 RPM and 55000 RPM. The introduction of vaned-diffuser losses requires to supply its main geometrical parameters, i.e. outlet and inlet diffuser angles ($\alpha_{3,bl}$, $\alpha_{4,bl}$), vane length and vane number (L_{vn}, N_{vn}), inlet and outlet vane thicknesses (t_3, t_4) and diffuser radial extensions (R_3, R_4). Although very detailed information about impeller geometry can be found in [7], only $\alpha_{3,bl} = 71.5°$ and $N_{vn} = 17$ are there clearly reported for the vaned diffuser. The missing geometrical information are retrieved from [21] (fig. 2, p. 3) by graphical extrapolation. Values adopted in the validation are: $t_3 = 1\,\text{mm}$, $t_4 = 6\,\text{mm}$, $R_3 \approx R_2$, $R_4 = 65.2\,\text{mm}$, $L_{vn} = 22.8\,\text{mm}$ and $\alpha_{4,bl} = 31.5°$. A relatively small outlet diffuser angle, measured from the radial direction, is consistent with the large volute size reported in [7]. Within this mean-line framework, the vaned diffuser and the volute are sized mainly according to Aungier [18]; for the volute, a circular external shape is assumed.

To foster the tool validity, an uncertainty-quantification analysis is also presented along with the validation. The scope is to prove that comparatively small variability in the input parameters does not produce large uncertainties in compressor performance, thus boosting the tool fidelity when different cases are compared. Moreover, unavoidable approximations in the derivation of the diffuser geometry are properly accounted in this way. A Monte Carlo sampling is performed for each rotational speed, including seven independent uncertainties as reported in Table 2. An uniform distribution is prescribed for all uncertainties. In addition to the geometrical data of the vaned diffuser, which were inferred from images reported in [21, 7], thus inherently uncertain, we also include the following uncertainties: the skin friction coefficient c_f, a coefficient k_μ which evaluates the effect of variations up to $\pm 2\%$ in the slip-factor estimation, and the design pressure-recovery coefficient for the vaned diffuser, defined as $C_P = (P_4 - P_3)/(P_{T3} - P_3)$, where the subscript T stands for total quantities.

Figure 2 reports the mean trend along with the extended confidence intervals for performance maps expressed in terms of total-to-static efficiency and enthalpy rise. This latter is intended as the equivalent enthalpy rise associated to the real increase in total pressure across the compressor, accordingly expressed as

$$h(P_{T5}, s_1) - h(P_{T1}, s_1) = l_{eul} - \Delta h_{imp} - \Delta h_{diff} - \Delta h_{vol}, \qquad (1)$$

where l_{eul} is the eulerian work, Δh_{imp} is the sum of all impeller losses, Δh_{diff} and Δh_{vol} includes all losses in the diffuser and volute, respectively. On the other hand, the compressor efficiency

This is a preprint of the following article: Romei, A., Gaetani, P., Giostri, A., & Persico, G., *The role of turbomachinery performance in the optimization of supercritical carbon dioxide power systems*, J. Turbomach., 2020.
The published article may differ from this preprint, and is available at the following DOI: 10.1115/1.4046182

Loss Mechanism	**Loss Model**	
Impeller incidence	$\Delta h_{in} = f_{inc}\, w_1^2 \sin^2(\beta_1 - \beta_{1,bl})$,	$f_{inc} = 0.5 \div 0.7$
Impeller blade loading	$\Delta h_{bl} = 0.05 D_f^2 u_2^2$,	$D_f = 1 - \frac{w_2}{w_1} + \frac{\Delta h_{TT}/u_2^2}{\frac{w_{1t}}{w_2}\left[\left(\frac{N_{eff}}{\pi}\right)\left(1 - \frac{D_{1t}}{D_2}\right) + 2\frac{D_{1t}}{D_2}\right]}$
Impeller clearance	$\Delta h_{cl} = 0.6 \frac{\delta_r}{b_2} v_{2,tg} \sqrt{\frac{4\pi(R_{1t}^2 - R_{1h}^2)\, v_{2,tg}\, v_{1,m}}{b_2 N_{eff}(R_2 - R_{1t})(1 + \rho_2/\rho_1)}}$,	
Impeller mixing	$\Delta h_{mx} = 0.5 \frac{v_2^2}{1 + \tan^2\alpha_2} \left(\frac{\varepsilon}{1-\varepsilon}\right)^2$,	$\varepsilon = 0 \div 0.35$
Impeller friction	$\Delta h_{sf} = 2 c_f \frac{L_b}{D_h} \overline{w}^2$,	$\overline{w} = \frac{v_{1,tg} + w_{1,tg} + v_2 + 2w_{1h} + 3w_2}{8}$
		$L_b = \frac{\pi}{8}(2R_2 - (R_{1t} + R_{1h}) - b_2 + 2L_{ax}) \left(\frac{2}{(\cos\beta_{1t} + \cos\beta_{1h})/2 + \cos\beta_{2,bl}}\right)$
		$L_{ax} = D_2(0.014 + 0.023\, D_2/D_{1h} + 2.012 \dot{V}_{T1}/(u_2 D_2^2))$
		$D_h = \frac{\pi(D_{1t}^2 - D_{1h}^2)}{2\pi D_1 + N_{eff}(D_{1t} - D_{1h})}$
Recirculation	$\Delta h_{rc} = 8 \times 10^{-5} \sinh(3.5\alpha_2^3) D_f^2 u_2^2$	
Disc friction	$\Delta h_{df} = c_f \frac{\overline{\rho} R_2^2 U_2^3}{4\dot{m}}$,	$\overline{\rho} = (\rho_2 + \rho_1)/2$
Leakage	$\Delta h_{lk} = \frac{\dot{m}_L u_L u_2}{2\dot{m}}$,	$\dot{m}_L = \rho_2 u_L \delta L_{ax} N_{eff}, \quad u_L = 0.816\sqrt{\frac{2\Delta P_L}{\rho_2}}$
		$\Delta P_L = \frac{\dot{m}(R_2 v_{2,tg} - R_{1t} v_{1t,tg})}{N_{eff} \overline{R} \overline{b} L_{ax}}, \quad \overline{R} = (R_2 + R_{1t})/2, \quad \overline{b} = (b_1 + b_2)/2$
Diffuser incidence	$\Delta h_{in,d} = f_{inc}\, v_3^2 \sin^2(\alpha_3 - \alpha_{3,bl})$,	$f_{inc} = 0.5 \div 0.7$
Diffuser friction	$\Delta h_{sf,d} = 2 c_f \frac{L_{vn}}{D_{h,vn} \delta_{BL}^{0.25}} \overline{v}^2$,	$\overline{v} = \sqrt{v_3^2 + v_4^2}/2$
		$L_{vn} = D_3(D_4/D_3 - 1)/(\cos\alpha_{3,bl} + \cos\alpha_{4,bl})$
		$\delta_{BL} = 5.142\, c_f L_{vn}/D_{h,vn}$
		$D_{h,vn} = (D_{3h} + D_{4h})/2$
		$D_{3h} = \frac{2b_2(2\pi R_3/N_{vn} - t_3)}{(\pi R_3/N_{vn} - t_3) + b_2/\cos\alpha_{3,bl}}, \quad D_{4h} = \frac{2b_2(2\pi R_4/N_{vn} - t_4)}{(\pi R_4/N_{vn} - t_4) + b_2/\cos\alpha_{4,bl}}$
Volute loss	$\Delta h_{vol} = \frac{v_{4,r}^2}{2}$	

TABLE 1: Loss correlations implemented in the centrifugal-compressor mean-line design tool. b: blade height, D: diameter, R: radius, δ_r: clearance thickness, ρ: density, v: absolute velocity, w: relative velocity, u: peripheral velocity, α: absolute flow angle, β: relative flow angle, $\dot{m}$: mass-flow rate, $\dot{V}$: volumetric-flow rate. $(\cdot)_1$: impeller inlet, $(\cdot)_2$: impeller outlet, $(\cdot)_3$: vaned diffuser inlet, $(\cdot)_4$: vaned diffuser outlet, $(\cdot)_5$: volute outlet, $(\cdot)_{bl}$: blade, $(\cdot)_t$: tip, $(\cdot)_h$: hub, $(\cdot)_{,tg}$: tangential, $(\cdot)_{,m}$: meridional, $(\cdot)_{,r}$: radial.

Uncertainty	**Range**	**Uncertainty**	**Range**
k_μ	$\mathscr{U}([0.98, 1.02])$	L_{vn}	$\mathscr{U}([22.4, 23.2])$ mm
c_f	$\mathscr{U}([0.005, 0.007])$	t_3	$\mathscr{U}([0.75, 1.25])$ mm
C_P	$\mathscr{U}([0.6, 0.7])$	t_4	$\mathscr{U}([5.75, 6.25])$ mm
		$\alpha_{4,bl}$	$\mathscr{U}([30, 35])^\circ$

TABLE 2: Uncertainties included in the validation process.

is generally defined in the code as

$$\eta_{T\chi}^c = \frac{h(P_{T5}, s_1) - h(P_{T1}, s_1) - \chi\, v_5^2/2}{l_{eul} + \Delta h_{ext}}, \tag{2}$$

where Δh_{ext} contains all external losses, while the definition of the parameter χ allows different efficiency formulations. If $\chi = 1$, the expression returns the total-to-static efficiency η_{TS}^c (as in the present validation case), while if $\chi = 0$, then it returns the total-to-total efficiency η_{TT}^c.

The validation shows that most of the experimental data fall

This is a preprint of the following article: Romei, A., Gaetani, P., Giostri, A., & Persico, G., *The role of turbomachinery performance in the optimization of supercritical carbon dioxide power systems*, J. Turbomach., 2020.
The published article may differ from this preprint, and is available at the following DOI: 10.1115/1.4046182

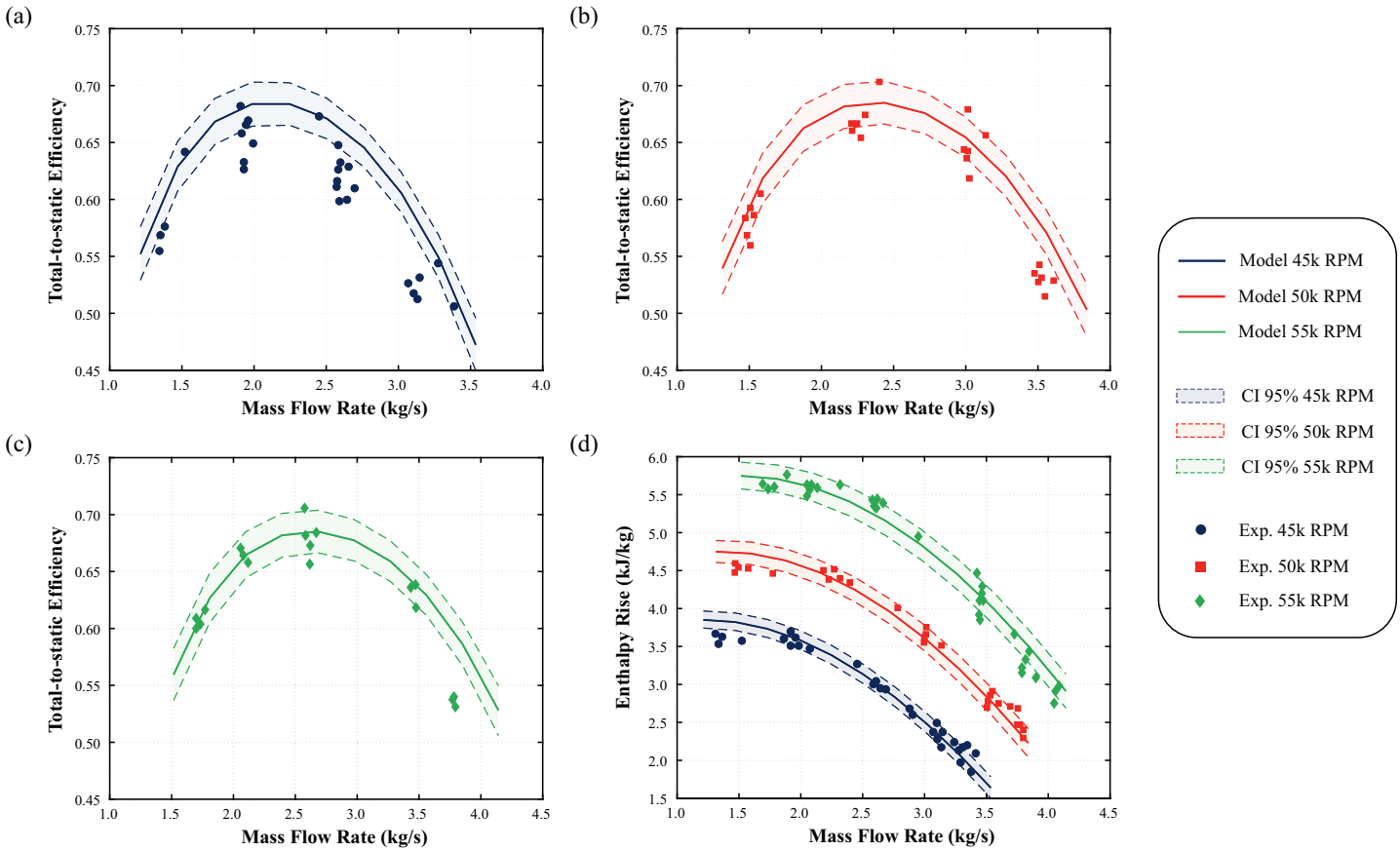

FIGURE 2: Compressor mean-line predictions along with 95% confidence intervals compared against experimental data [7]. Efficiency maps for (*a*) 45000 RPM, (*b*) 50000 RPM and (*c*) 55000 RPM. Enthalpy-rise map at different speedlines in subfigure (*d*).

in the predicted 95% confidence intervals. A slightly higher discrepancy (≈ 1%pts) is found in the efficiency maps for the lowest rotational speed. Moreover, upon examination of Figures 2(*a*)–(*c*), the mean-line code overpredicts the efficiency at higher flow coefficients. The enthalpy-rise map, on the other hand, perfectly matches experimental data for all rotational speeds and flow coefficients. The combination of efficiency and enthalpy-rise maps suggests that the overprediction in the efficiency curves at higher flow coefficients can be attributed either to the outlet kinetic energy or to the external losses, by comparison of their associated formulations (see Eqs. (1) and (2)). Nonetheless, we will only refer to the peak (design) efficiency; accordingly, the overprediction at higher flow coefficients does not undermine the validity of results presented in the following. Finally, the uncertainty in the efficiency prediction is around ± 1.5%pts for peak values, which is satisfactory in light of the large uncertainties characterizing the diffuser geometry.

1.3 Mean-line tool for axial turbines

The design of sCO_2 turbines is performed by using the in-house mean-line code zTurbo [22]. zTurbo was conceived for the design of different turbine architectures, operating in subsonic, transonic or supersonic flow regimes. Like any mean-line models, zTurbo inherently ignores the detailed shape of the turbine blades, but it relies on correlations for losses whose reliability determines the fidelity of the performance estimates. Few studies document a good agreement between the mean-line calculations and performance measurements [23, 24].

Within the framework of zTurbo, the calculation is run assigning total quantities at the turbine inlet, the static pressure at the outlet, and the mass-flow rate along with the main geometrical parameters. The code contains several loss correlations, e.g. Ainley & Mathieson, Traupel, and Craig-Cox for axial turbines, complemented by specific corrections for supersonic flows and post-expansions downstream of the throat. In this work, Traupel loss correlations are employed. The outflow angle is estimated by applying a proper deviation correlation [25], while the blade number is evaluated with the standard loading criterion of Zweifel [26].

In the last five years, zTurbo was applied to axial [27, 28], radial-outflow [29, 28], and radial-inflow [28] turbines. Casati *et al.* [27] reports a validation against a four-stage axial turbine, showing prediction capabilities similar to what documented in [30] (namely, errors of ≈ 2%pts with respect to the experiments).

This is a preprint of the following article: Romei, A., Gaetani, P., Giostri, A., & Persico, G., *The role of turbomachinery performance in the optimization of supercritical carbon dioxide power systems*, J. Turbomach., 2020.
The published article may differ from this preprint, and is available at the following DOI: 10.1115/1.4046182

2 OPTIMAL COMPRESSOR DESIGN AT VARIABLE OPERATING POINT, SIZE AND PRESSURE RATIO

The aim of this section is to assess the implication of the so-called real-gas effects, depending on the upstream thermodynamic state, on the achievable compressor efficiency η^c_{TT} for different sizes and pressure ratios. To this end, several optimizations are carried out in order to generate optimized compressor designs (in terms of highest total-to-total efficiency) by varying the inlet thermodynamic states and, consequentially, the departure from the ideal-gas approximation (see, e.g., the compressibility factor map in Figure 1). Representative 26 compressor-intake conditions are recognized in the plane T–s (identified by black dots in Figure 3) in the range of $33\,^\circ\text{C} < T_{T1} < 150\,^\circ\text{C}$ and $70\,\text{bar} < P_{T1} < 100\,\text{bar}$. The lower temperature limit is chosen to avoid local two-phase flows in the compressor (at least in design conditions), while the upper limit eventually includes realistic inlet conditions for the recompressor. Pressure limits are based on preliminary cycle considerations for different minimum temperatures, retaining a large range to widen the analysis.

Several assumptions for the compressor design are made: (i) the impeller blade number is computed as in [31]; (ii) splitter blades are included; (iii) zero incidence is assigned at the impeller inlet; (iv) no purely radial impeller geometry is considered; (v) the vaned-diffuser is designed (L_{vn}, N_{vn}, R_3, R_4) according to Aungier [18]; (vi) the diffuser inlet flow angle is not corrected for the diffusion in the vaneless space; (vii) the pressure-recovery coefficient C_P is set at 0.7, which is representative of a fair diffusion process in design conditions; (viii) blade and vane thicknesses are proportionally scaled from the Sandia's main compressor; (ix) clearances are proportionally scaled from the Sandia's main compressor, considering a maximum cap of 1 mm.

The user cannot arbitrarily impose the target pressure ratio, but it results from the mean-line calculations (only inlet total conditions are imposed). Therefore, a penalty formulation is embedded in the objective function (η^c_{TT}) to drive the optimization towards designs satisfying the prescribed pressure ratio, accepting an absolute error of 0.01. Moreover, since the aim of the designer is to avoid choked-flow operations at least in the design condition, neither in the impeller nor in the diffuser, both relative Mach number at the impeller inlet and absolute Mach number at the impeller outlet are constrained, $M_{w1t} < 1.3$ and $M_2 < 1.1$ respectively. This latter parameter is still consistent with unchoked operations since the vaneless gap between the impeller and the vaned diffuser can be properly sized to avoid the onset of sonic throats within the vaned-diffuser channel. Design variables for the optimizations are reported in Table 3. The lower and upper bounds are based on aerodynamic and rotordynamic considerations, whose explanation can be found in several textbooks (see, e.g., [32, 33]). Preliminary optimization tests unveiled the pres-

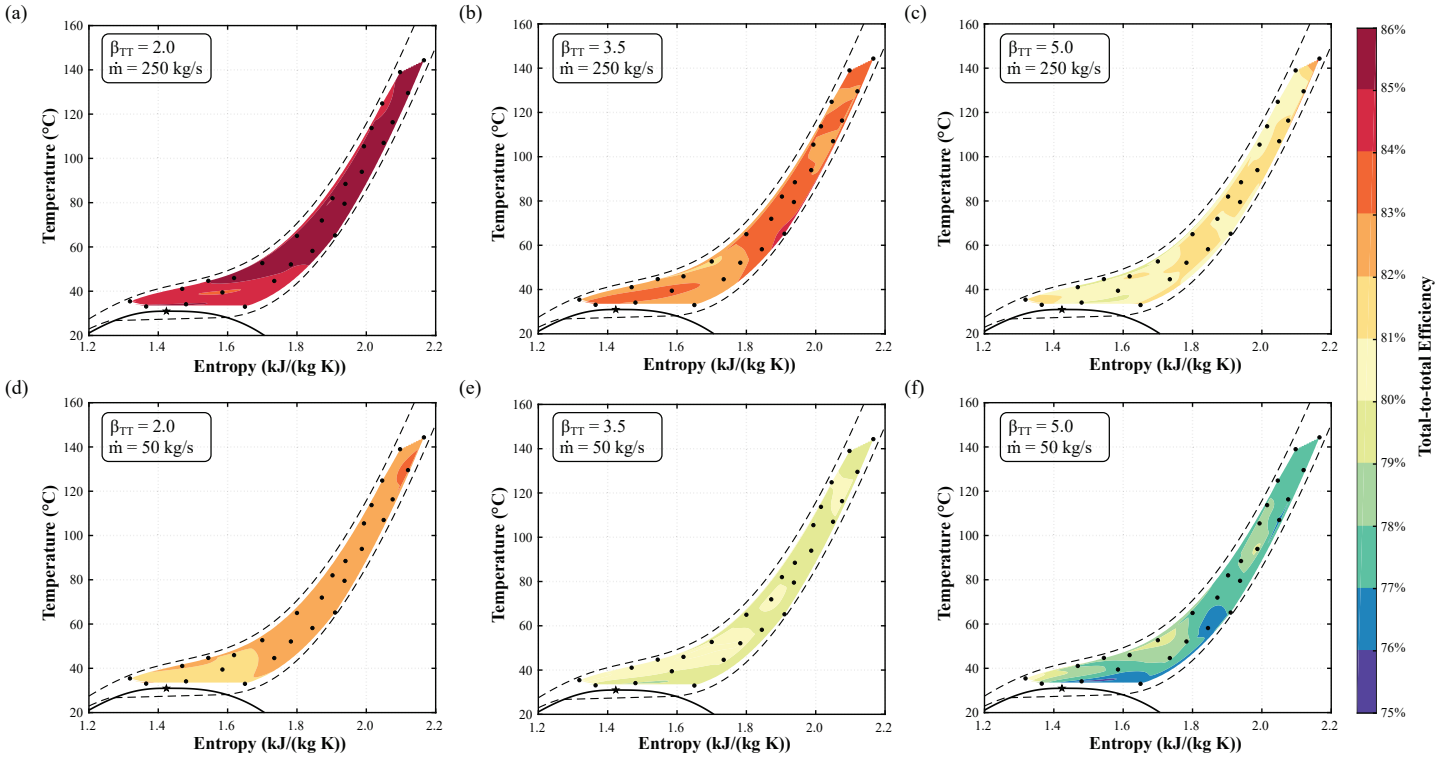

FIGURE 3: Compressor total-to-total efficiency η^c_{TT} contours on the T–s thermodynamic plane for different pressure ratios and mass flow rates. (- - -) minimum (70 bar) and maximum (100 bar) isobars; (•) inlet thermodynamic states on which the optimization is performed. ($\star$) CO_2 critical point ($T_c = 30.98\,^\circ\text{C}$, $P_c = 73.77\,\text{bar}$).

This is a preprint of the following article: Romei, A., Gaetani, P., Giostri, A., & Persico, G., *The role of turbomachinery performance in the optimization of supercritical carbon dioxide power systems*, J. Turbomach., 2020.
The published article may differ from this preprint, and is available at the following DOI: 10.1115/1.4046182

Design Variable	Lower bound	Upper bound
$\phi = \dot{V}_{T1}/(u_2 D_2^2)$	0.02	0.09
N	2000 RPM	100 000 RPM
$k = 1 - D_{1h}^2/D_{1t}^2$	0.5	0.95
$\beta_{2,bl}$	-70°	-10°
$\alpha_{3,bl}$	65°	75°
b_2/D_2	0.03	0.08
D_{1t}/D_2	0.3	0.7
$AR = [R_4 \cos(\alpha_{4,bl})]/[R_3 \cos(\alpha_{3,bl})]$	1	3

TABLE 3: Design variables for the optimization of centrifugal compressors.

ence of multiple local optima, thus excluding gradient-based optimization methods. Therefore, optimization problems are solved with genetic algorithms available in the Optimization Toolbox of Matlab®. As these algorithms are meta-heuristic, five optimizations are performed for each inlet condition. The compressor design with the maximum objective-function value out of the five trials is ultimately selected.

Two compressor sizes are considered, induced by two representative values of the ingested mass-flow rate. According to Crespi *et al.* [6], the net specific work for a recompression cycle is typically in the range of $75 \div 175\,\mathrm{kJ/kg}$. Considering as spectrum of power $5 \div 50\,\mathrm{MW}$, the turbine mass-flow rate is in the range of $70 \div 300\,\mathrm{kg/s}$. As long as both the main compressor and the recompressor elaborate only a part of the total mass-flow rate, the analysis is performed for $\dot{m} = 50\,\mathrm{kg/s}$ and $\dot{m} = 250\,\mathrm{kg/s}$. Mass-flow rates below $\dot{m} = 50\,\mathrm{kg/s}$ are not considered, because the resulting compressor size would be so small to make the rotordynamics, sealing and bearing features dominate over the aerodynamics. Finally, three representative pressure ratios $\beta_{TT} = P_{T5}/P_{T1}$ are investigated, namely 2, 3.5 and 5. Higher pressure ratios are excluded from the analysis because they lead to technically not-relevant maximum pressure ($> 450\,\mathrm{bar}$).

The maximum compressor efficiencies for the combination of selected pressure ratios, mass-flow rates and inlet thermodynamic conditions are conveniently reported in the T–s diagram in Figure 3. The efficiency fields indicate that a specific pattern connected to the inlet thermodynamic conditions cannot be easily recognized. Although at low pressure ratios a difference between comparatively low and high temperature is present, see Figures 3(*a*) and 3(*d*), the variation is relatively low (≈ 1%pts) and probably included in the computational uncertainty. Still, an opposite trend is observed in Figure 3(*e*), where the compressor presumably works less efficiently when the inlet thermodynamic conditions are far from the critical ones. The present analysis, given the design assumptions, seems to suggest that the compressor-intake thermodynamic conditions have no relevant consequences on the achievable compressor efficiency, but comparable efficiencies can be obtained after a dedicated optimization task. The resulting optimized compressor layouts are shown for two representative intake conditions in Figure 4, taking as a reference the smallest mass-flow rate. The first set of thermodynamic conditions ($T_{T1} = 34\,^\circ\mathrm{C}$, $P_{T1} = 78.75\,\mathrm{bar}$, $\rho_{T1} = 447.81\,\mathrm{kg/m^3}$) leads to a density which is approximately four times higher than the second one ($T_{T1} = 145\,^\circ\mathrm{C}$, $P_{T1} = 74.00\,\mathrm{bar}$, $\rho_{T1} = 105.4\,\mathrm{kg/m^3}$).

At first glance, the most evident geometrical difference lies in a bigger impeller-eye opening and volute to compensate the overall lower density. However, a more careful inspection reveals that flow evolutions along the impeller meridional coordinate are relatively different. Compressors designed for upstream thermodynamic conditions far from the critical point show a sharper variation in the blade height across the impeller. In fact, when the volumetric variation ($\dot{V}_{5,is}/\dot{V}_{T1}$) is considered, the first set of operating conditions shows 0.77 and 0.62 for $\beta_{TT} = 2$ and $\beta_{TT} = 5$, respectively. Conversely, the second set shows 0.59 and 0.32 for the same pressure ratios. The difference in the volumetric behaviour for the same pressure ratio can be explained only as a contribute of real-gas effects, enhanced in the first case due to the proximity of the thermodynamic inlet conditions to the critical point. To be more specific, by comparing the previous results obtained for $T_{T1} = 34\,^\circ\mathrm{C}$ and $P_{T1} = 78.75\,\mathrm{bar}$ with the ones obtained in the ideal-gas limit (i.e. low pressures and high temperatures), there is an underestimation of the volumetric variation of 24% for $\beta_{TT} = 2$, which increases to 53% for $\beta_{TT} = 5$. These errors have to be compared with the one made by using an ideal-gas model to estimate the flow evolution for the second set of inlet thermodynamic conditions, resulting to 0.7% for $\beta_{TT} = 2$ and 9% for $\beta_{TT} = 5$. It follows that accounting for real-gas properties is crucial to obtain a reliable preliminary design of the machine when it operates in the neighbourhood of the thermodynamic critical point. Moreover, this analysis demonstrates that the op-

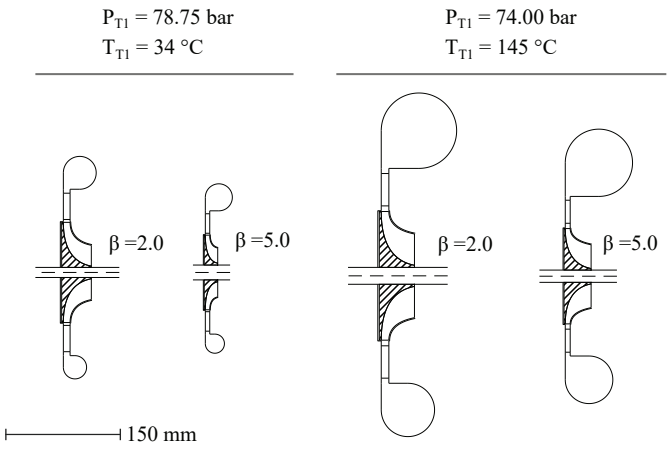

FIGURE 4: Optimal compressor layouts for different intake-fluid thermodynamic conditions. The mass-flow rate is $50\,\mathrm{kg/s}$ for all compressors represented in the figure.

This is a preprint of the following article: Romei, A., Gaetani, P., Giostri, A., & Persico, G., *The role of turbomachinery performance in the optimization of supercritical carbon dioxide power systems*, J. Turbomach., 2020.
The published article may differ from this preprint, and is available at the following DOI: 10.1115/1.4046182

timization of the mean-line code converges to the proper geometry by considering the meridional flow-path evolution. Finally, it is possible to achieve technically-competitive compressor efficiencies, comparable to those obtained in more dilute condition (where the ideal-gas behaviour is partially recovered), when designing representative full-scale compressors.

With reference to Figure 3, the mass-flow rate (i.e. the compressor size) or the pressure ratio (i.e. the compressor loading) show larger effects on the compressor efficiency. On the one hand, the size reduction, e.g. from Figure 3(*a*) to Figure 3(*d*), causes a clear efficiency reduction ($\Delta\eta^c_{TT} \approx -2.5$%pts), due to the increase in the clearance- and leakage-loss relative weight. This efficiency decrement given by size effects ($\Delta\eta^c_{TT} \approx -2 \div 3$%pts) is found at each pressure ratio of the present analysis. On the other hand, by increasing the pressure ratio, hence the aerodynamic loading and its associated losses (e.g. blade loading and recirculation), the compressor efficiency drops about 2%pts as well. Moreover, the same qualitative behaviour given by a pressure-ratio variation is found for the two ingested mass-flow rates, not evidencing an explicit cross-dependency between aerodynamic loading and compressor size.

As far as optimal rotational speeds are concerned, they show a wide range of variation within the limits selected for the optimizations. To give an overview, we refer to the extreme cases, i.e. the smallest highly-loaded compressor ($\dot{m} = 50\,\mathrm{kg/s}$, $\beta_{TT} = 5$) and the largest slightly-loaded compressor ($\dot{m} = 250\,\mathrm{kg/s}$, $\beta_{TT} = 2$). The former features optimal rotational speeds in the order of $60\,000 \div 80\,000$ RPM within the investigated thermodynamic ranges, while the latter shows comparatively smaller values and range ($10\,000 \div 20\,000$ RPM). The imposition of a lower rotational speed, for example employing a single-shaft configuration, would presumably result in a much lower compressor efficiency with respect to those reported in this work. Finally, for all examined cases, the peripheral velocity is found to be lower than $500\,\mathrm{m/s}$, thus limiting eventual issues related to the mechanical integrity.

3 TURBOMACHINERY-EFFICIENCY CORRELATIONS

In this section, efficiency correlations to be included in the cycle analysis are devised. We initially limit our analysis to single-stage turbomachinery, since the relatively limited pressure ratio of interest to sCO_2 cycles ($\sim 2 \div 5$) can be disposed efficiently with a single-stage configuration for both centrifugal compressors and axial turbines, thus guaranteeing a relevant technical simplification. If the cycle is intended for power capacity higher than approximately 100 MW, multi-stage turbomachinery becomes the only viable choice capable of elaborating the large flow rates while exhibiting comparatively higher component efficiencies. In the last section of the paper, an extension to multi-stage architectures is discussed, still focusing on relatively small power targets.

Recalling the approach of Macchi & Perdichizzi [34], both compressor and turbine efficiencies are expressed as function of two independent similarity parameters. The selected parameters are the pressure ratio β, which accounts for machine loading, and the size parameter SP, which includes size effect. As a matter of fact, self-similarity in Reynolds number can be assumed, since the Reynolds number exceeds 10^7 for both the machines in the conditions of interest. Besides, the impact of the fluid thermodynamics is neglected as the fluid does not change and the optimal turbomachinery efficiency was demonstrated not to depend on the intake conditions. Finally, as the correlations are calibrated on already optimized turbomachinery, a parameter accounting for the rotational speed is not needed [35] (turbomachinery are supposed to work at their optimal rotational speed). It follows that the implementation of these correlations to estimate optimized turbomachinery efficiencies within cycle routines implicitly assumes that each turbomachinery rotates at its own optimal rotational speed on separate shafts. Size parameter SP and the pressure ratio β are declined differently if referring either to the compressor or to the turbine:

$$\text{compressor:} \quad \beta_c = \frac{P_{T,out}}{P_{T,in}}, \qquad SP_c = \frac{\sqrt{\dot{V}_{T,in}}}{\Delta h_{is}^{0.25}}, \tag{3}$$

$$\text{turbine:} \quad \beta_t = \frac{P_{T,in}}{P_{out}}, \qquad SP_t = \frac{\sqrt{\dot{V}_{out,is}}}{\Delta h_{is}^{0.25}}, \tag{4}$$

where the subscript T stands for total quantities, while the subscript *is* indicates that the quantity is obtained through an isentropic process.

These two parameters allow a straightforward implementation within cycle routines, without significantly increasing the computational cost. Different analytical formulations (exponential, cubic, quadratic, polynomial) were tried to properly interpolate the evolution of turbomachinery efficiencies when the size parameter and the pressure ratio are varied. Eventually, we select the simple yet effective polynomial formulation,

$$\eta = a\,SP^b + c\,\beta^d + e, \tag{5}$$

where a, b, c, d, e are determined via a least-square regression of optimized turbomachinery designs. For both the correlations, the maximum deviation between the predicted and the actual (as provided by the mean-line optimization) value are reported. Moreover, the coefficient of determination R^2, whose standard definition is reported as follows, is evaluated for both cases.

$$R^2 = 1 - \frac{\sum_{i=1}^{N}(\eta_i - \hat{\eta}_i)^2}{\sum_{i=1}^{N}(\eta_i - \overline{\eta})^2}, \tag{6}$$

where N is the number of optimized designs considered for the correlation fitting, η_i are the efficiency values provided by the mean-line code optimization, $\overline{\eta}$ is their mean value and $\hat{\eta}_i$ are the values predicted by the correlation.

This is a preprint of the following article: Romei, A., Gaetani, P., Giostri, A., & Persico, G., *The role of turbomachinery performance in the optimization of supercritical carbon dioxide power systems*, J. Turbomach., 2020.
The published article may differ from this preprint, and is available at the following DOI: 10.1115/1.4046182

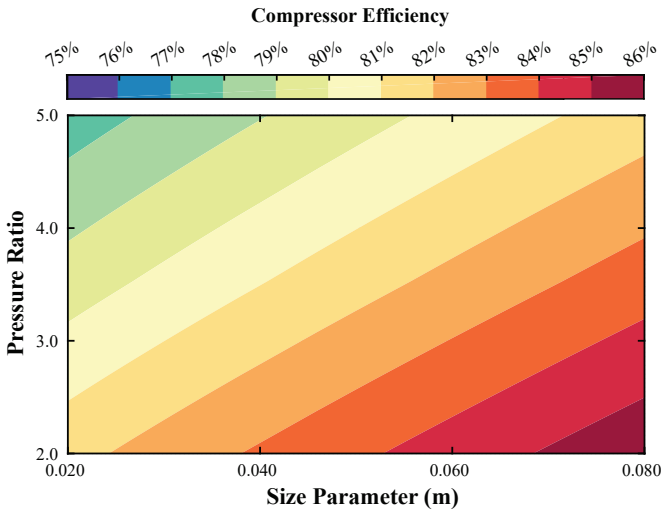

FIGURE 5: Compressor total-to-total efficiency η^c_{TT} as a function of size parameter SP_c and pressure ratio β_c.

3.1 Compressor-efficiency correlation

The centrifugal-compressor efficiency correlation is formulated by including all the optimal compressor designs presented in Section 2, consisting in overall $N = 156$ designs. About 8% of the optimal compressor pool exhibits a discrepancy of $1.0 \div 2.0$%pts with respect to the predicted efficiency value. These deviations are considered acceptable because they are within the uncertainty range of the mean-line tool. One outlier ($|\eta - \hat{\eta}| = 3$%pts) is noticed and excluded a posteriori from the fitting. The final compressor-efficiency correlation, reported graphically in Figure 5, reads as

$$\eta_c = 0.4649\, SP_c^{0.8033} - 0.0183\, \beta_c^{0.8870} + 0.8298. \tag{7}$$

The validity ranges for such correlation are $2 \leq \beta_c \leq 5$ and $0.020\,\text{m} \leq SP_c \leq 0.080\,\text{m}$. The coefficient of determination is $R^2 = 0.87$. Reasonably, the predicted efficiency can be clipped for $SP_c > 0.080\,\text{m}$, assuming that size effects are going to vanish as compressor size increases.

3.2 Turbine-efficiency correlation

Before illustrating the turbine-efficiency correlation, the optimization set-up is discussed. Some design assumptions are made in this context: (i) pure axial flow at the stator inlet; (ii) constant mean diameter; (iii) the stator-rotor axial distance is set as 0.5 of the stator axial chord; (iv) trailing-edge thickness-to-throat opening ratio is set at 0.1 for both stator and rotor; (v) stator hub and rotor tip clearances are equal to 0.5 mm. Design variables are instead reported in Table 4. As for compressor optimizations, lower and upper bounds are chosen accordingly to aerodynamic and mechanical considerations available in Open Literature.

The objective function is the maximization of machine efficiency, which is generally coded in zTurbo as

$$\eta^t_{T\chi} = \frac{l_{eul}}{h_{T1} - h_{3,is} - \chi v_3^2/2}. \tag{8}$$

Depending on how much kinetic energy $v_3^2/2$ is recovered downstream of the turbine, different efficiency formulations are possible. We assume that a diffuser is installed downstream of the turbine, recovering 50% of the residual kinetic energy, hence $\chi = 0.5$ is used for the turbine efficiency hereinafter.

The objective function accounts for different penalties if some design constrains are not satisfied. In particular, we impose that: (i) the flaring angle, both for the stator and the rotor, cannot exceed $\pm 15°$; (ii) the absolute Mach number downstream of the stator M_1 has to be lower than 1.35 (eventually relying on supersonic post-expansion, which becomes too inefficient for $M_1 > 1.4$); (iii) the peripheral speed at midspan cannot exceed 500 m/s. The expected presence of multiple local maxima drives the choice of the optimization algorithm towards meta-heuristic methods as for the compressor optimizations. To reduce the possible stochastic scatter given by meta-heuristic methods, each optimization is run twice and the best design in terms of highest turbine efficiency is selected.

As the turbine-intake thermodynamic conditions in the range of interest for sCO_2 power systems are not expected to trigger peculiar real-gas effects, a comparatively lower number of optimizations is performed. We identify $N = 36$ optimal designs in the range of $\dot{m} = 50 \div 250\,\text{kg/s}$, $T_{T0} = 550 \div 750\,°\text{C}$ and $\beta_t = 2 \div 5$. Additional optimizations are run for $\dot{m} > 250\,\text{kg/s}$, evidencing no efficiency variations given the other two parameters constant. For all turbine designs, the reaction degree r,

Design Variable	Lower bound	Upper bound
N	2000 RPM	100 000 RPM
α_1	65 °	78 °
c_s	20 mm	100 mm
β_3	65 °	78 °
c_r	20 mm	100 mm
b_0	10 mm	50 mm
b_0/D_m	0.025	0.25
$r = (h_{1,is} - h_{3,is})/(h_{T0} - h_{3,is})$	0	0.8

TABLE 4: Design variables for the optimization of single-stage axial turbine. N: rotational speed; α: absolute flow angle; β: relative flow angle; c: axial chord; b: blade height; D: diameter; r: reaction degree; $(\cdot)_0$: stator inlet; $(\cdot)_1$: stator outlet; $(\cdot)_2$: rotor inlet; $(\cdot)_3$: rotor outlet; $(\cdot)_s$: stator; $(\cdot)_r$: rotor; $(\cdot)_m$: midspan; $(\cdot)_{is}$: isentropic; $(\cdot)_T$: total quantity.

This is a preprint of the following article: Romei, A., Gaetani, P., Giostri, A., & Persico, G., *The role of turbomachinery performance in the optimization of supercritical carbon dioxide power systems*, J. Turbomach., 2020.
The published article may differ from this preprint, and is available at the following DOI: 10.1115/1.4046182

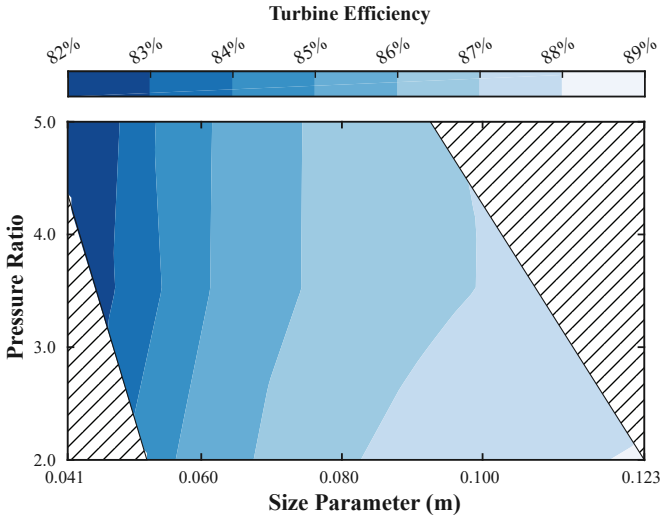

FIGURE 6: Turbine efficiency $\eta^t_{T\chi}$, with $\chi = 0.5$, as a function of size parameter SP_t and pressure ratio β_t. The correlation is not valid within dashed areas.

defined as in Table 4, results approximately 0.5. At the lowest mass-flow rate, i.e. $\dot{m} = 50\,\mathrm{kg/s}$, the rotational speed is found at its upper limit (100 000 RPM), suggesting that the optimal rotational speed may be beyond that value. All other optimal designs are characterized by rotational speeds between $20\,000 \div 95\,000$ RPM, typically higher than their compressor counterparts. If a single-shaft compressor-turbine configuration is desired, a trade-off on the rotational speed should be made, compromising at least one out of two machine performance.

As in the previous section, the turbine-efficiency correlation is obtained by fitting the efficiency of these representative 36 optimal designs. The maximum deviation between the mean-line efficiency and the predicted value is below 1%pts for all examined cases. No outliers are found. The coefficient of determination is $R^2 = 0.96$. The analytical expression reads as

$$\eta_t = -0.0003\, SP_t^{-1.7107} + 5.0665\, \beta_t^{-9.7428} + 0.8858, \quad (9)$$

whose validity range is reported in Figure 6. The correlations can be clipped for size parameters SP beyond the upper limit, as optimization tests for higher flow rates demonstrated self-similarity for size effects.

4 sCO_2 CYCLE OPTIMIZATIONS ACCOUNTING FOR TAILOR-MADE TURBOMACHINERY EFFICIENCY

A dedicated analysis on sCO_2 cycle optimizations, including a proper modelling of turbomachinery efficiencies, is now presented. The investigation is limited to the recompression sCO_2 cycle, under the assumptions presented in the Section 1.1, at full-load condition. However, since the backbone of sCO_2 power cycles is invariant among different layouts, we expect that the present findings are not limited to the cycle arrangement here considered.

The main goal of this study is to analyse the impact of the turbomachinery efficiencies on cycle performance estimates; in particular, the proposed correlations are compared to the standard assumptions of taking fixed turbomachinery efficiencies. The assessment is carried out in parametric way, by changing the hot-source temperature (T_{max}), the cycle minimum temperature (T_{min}) and the net power output ($\dot{W}_{el}$). Varying the cycle pressure ratio (i.e. ratio between cycle maximum and minimum pressure) within the range of validity of the proposed correlations (i.e. $\beta = 2 \div 5$), the sCO_2 cycle is optimized in terms of cycle electrical efficiency, taking as design variables the minimum pressure and the split factor. Note that each turbomachinery features slightly different pressure ratios as a consequence of the pressure drops occurring in the heat exchangers.

Three turbomachinery models are tested: (i) constant-turbomachinery efficiencies $\eta_t = 0.90$ and $\eta_c = 0.86$; (ii) constant-turbomachinery efficiencies $\eta_t = 0.86$ and $\eta_c = 0.82$; (iii) turbomachinery-efficiency correlations $\eta = f(SP, \beta)$, as formulated in Section 3. The first set of constant efficiencies represents relatively optimistic designs and they are approximately comparable with values presently adopted for gas-turbine applications. On the other hand, the second set exhibits more realistic values, taken approximately as the mean values provided by the correlations given in Equations (7) and (9).

First, the hot-source temperature is changed and the related variations on cycle performance are analysed by employing different fidelity models for the turbomachinery components. The cycle minimum temperature and the power size are set constant at $T_{min} = 35\,^\circ\mathrm{C}$ and $\dot{W}_{el} = 25\,\mathrm{MW}$, respectively. Two maximum temperature values are considered, namely $T_{max} = 550\,^\circ\mathrm{C}$ and $T_{max} = 750\,^\circ\mathrm{C}$. The results of this analysis are illustrated in Figure 7(*a*). Qualitatively, the efficiency trends for both hot-source temperatures are similar. From a quantitative perspective, instead, there is ≈ 10%pts-difference in the efficiency value between the lowest and the highest hot-source temperature. This difference is expected as the maximum temperature has a significant influence on the overall cycle efficiency. When $\beta = 2$, the optimized electrical efficiency including turbomachinery-efficiency correlations is similar to the one predicted with the first set of constant-turbomachinery efficiencies (i.e. $\eta_t = 0.90$ and $\eta_c = 0.86$). Coherently, at low pressure ratio and moderate power size, the predicted turbomachinery efficiencies from the two models are found comparable. Nevertheless, as long as the pressure ratio increases, the discrepancy between two models increases as well. Constant-efficiency models only show the thermodynamic impact of the pressure ratio on the cycle, without accounting for the impact of the increased aerodynamic loading on the turbomachinery performance. At about $\beta = 3.5$, turbomachinery efficiencies predicted via correlations are approximately equal to the second set of constant-efficiencies ($\eta_t = 0.86$ and $\eta_c = 0.82$). At higher pressure ratio, the efficiency penalty increases and the overall cycle efficiency starts decreasing, evidencing a maximum in the curve $\eta_{el}(\beta)$ for both the hot-source

This is a preprint of the following article: Romei, A., Gaetani, P., Giostri, A., & Persico, G., *The role of turbomachinery performance in the optimization of supercritical carbon dioxide power systems*, J. Turbomach., 2020.
The published article may differ from this preprint, and is available at the following DOI: 10.1115/1.4046182

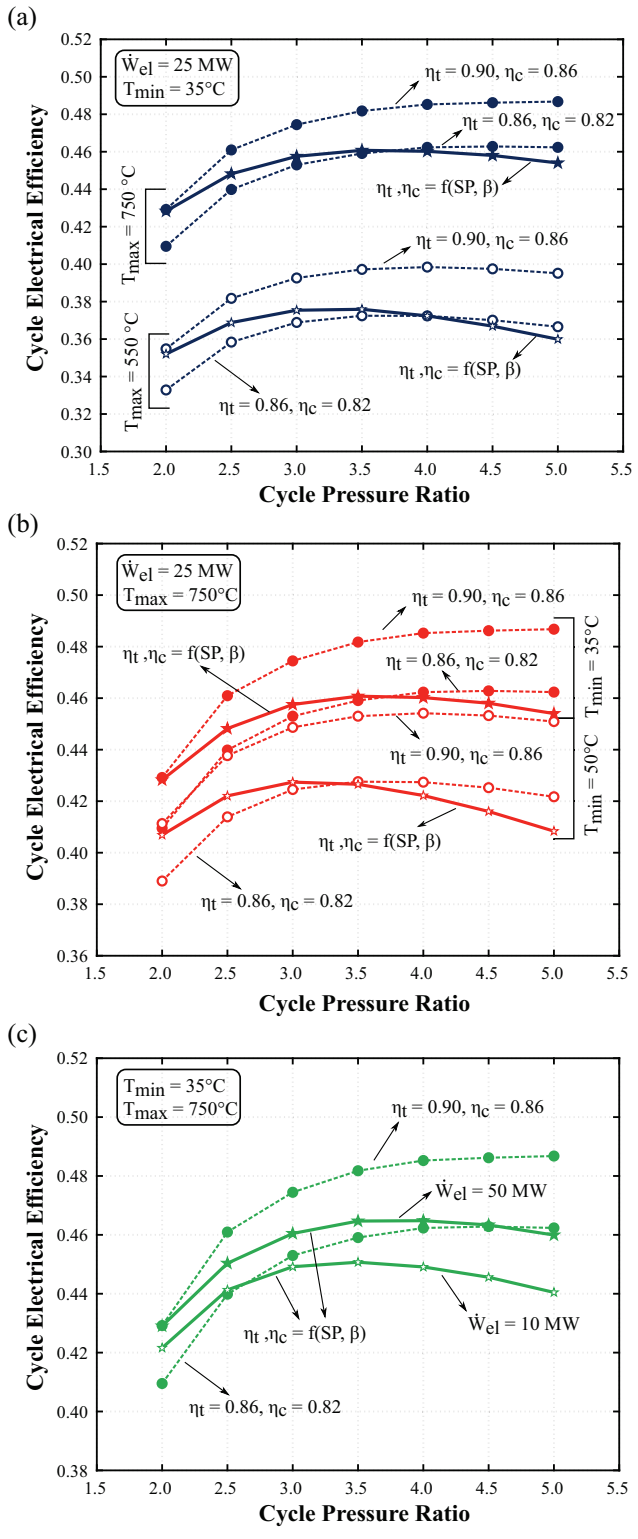

FIGURE 7: Parametric assessment of cycle efficiency η_{el} evolution as a function of the cycle pressure ratio P_{max}/P_{min} by changing the hot-source temperature (*a*), the minimum temperature (*b*) and the installed power capacity (*c*).

temperatures. In absence of proper correlations for the turbomachinery efficiency, the maximum is not captured at the highest hot-source temperature, while a slight reduction of electrical efficiency can be appreciated at the lowest maximum temperature. However, for this latter case, the reduction in the cycle performance is only given by the smaller fraction of residual heat available at the turbine outlet, which affects the recuperative process, and not also by the deterioration of turbomachinery performance. Indeed, the cycle efficiency drop is more pronounced when turbomachinery-efficiency correlations are employed, because two effects (lower turbomachinery efficiency and worse recuperative process) couple to decrease the cycle efficiency. An increase of the maximum temperature hides the second effect when $\beta < 5$, resulting not only to a quantitative overestimation of the overall cycle efficiency but also to a wrong trend prediction when constant efficiencies are assumed. At the highest pressure ratio, which represents the worst-case scenario where larger efficiency differences are found, cycle efficiency is overestimated of about 1.0%pts and 4.0%pts by employing the two set of constant efficiencies with respect to the prediction provided by using correlations.

Figure 7(*b*) shows the effect of the minimum temperature, by keeping constant the hot-source temperature and the power capacity at $T_{max} = 750\,°C$ and $\dot{W}_{el} = 25\,MW$, respectively. The main trend of electrical efficiency is qualitatively similar to the ones observed in the previous analysis. When the minimum temperature increases, the overall lower cycle efficiency is related to the higher compression work required by the main compressor. This latter evidence can also explain why the optimal pressure ratio is different for the two cases when the efficiency correlations are used. Indeed, the reduction of the main-compressor efficiency given an increase of the pressure ratio affects more the cycle efficiency, as a consequence of the larger work required to compress CO_2 far from the critical point.

Finally, the implications of a small power capacity on the cycle efficiency are illustrated in Figure 7(*c*). It compares the variation of cycle efficiency with the pressure ratio for two representative plant capacities, namely 10 MW and 50 MW. The minimum and maximum temperature are equal to $T_{min} = 35\,°C$ and $T_{max} = 750\,°C$. By applying constant efficiency for the turbomachinery, the cycle performance are not dependent on the plant size; indeed, cycle routines can be equivalently formulated in terms of specific quantities. On the other hand, considering the performance of turbomachinery within the cycle routines, appreciable differences are found. The smaller plant size has an efficiency which is lower of around 1%pts at small pressure ratio up to 2%pts when $\beta = 5$ if compared to the larger plant capacity. This efficiency deviation between the two plant capacities is only related to the corresponding turbomachinery size, accounted in the size parameters within the correlations (see Equations (7) and (9)).

To sum up, for all the investigated parametric cases, a noticeable difference is found in the prediction of cycle efficiencies and of optimal pressure ratios, when a proper turbomachinery modelling is included in the cycle analyses. A set of constant

This is a preprint of the following article: Romei, A., Gaetani, P., Giostri, A., & Persico, G., *The role of turbomachinery performance in the optimization of supercritical carbon dioxide power systems*, J. Turbomach., 2020.
The published article may differ from this preprint, and is available at the following DOI: 10.1115/1.4046182

efficiencies, which may be of general validity and can provide comparably accurate results (i.e. within 2%pts with respect to the correlations) for all examined ranges, i.e. $T_{max} = 550 \div 750\,°C$, $T_{min} = 35 \div 50\,°C$ and $\dot{W}_{el} = 10 \div 50\,MW$, seems not to be available.

5 POTENTIAL EFFICIENCY GAIN EMPLOYING MULTI-STAGE TURBOMACHINERY

Up to this point, we limited the investigation on cycle performance to single-stage turbomachinery. However, multi-stage arrangements might exhibit higher efficiencies as a consequence of the reduced aerodynamic loading at high cycle pressure ratio and/or in connection to technological constraints in terms of angular or peripheral speed. The aim of this section is to asses the potential efficiency gain achievable through multi-stage turbomachinery with respect to single-stage configurations.

To this end, several optimizations, for both two-stage centrifugal compressors and axial turbines, are performed for a discrete number of pressure ratios and size parameters. The optimization algorithm, as well as the optimization set-up in terms of objective functions, constraints and design variables, recalls the one discussed for the optimizations of the corresponding single-stage layout. The geometrical design variables, see Tables 3 and 4 for compressors and turbines, respectively, are doubled (one group for each stage), while the same rotational speed is considered for both stages. Besides, the pressure-ratio distribution between the two stages is also optimized, retaining that their product must satisfy the overall prescribed pressure ratio. As far as the multi-stage centrifugal compressor is concerned, the crossover bend and the return vane channel, which deswirles the flow before entering into the next impeller, deserve appropriate considerations. Under the assumption of zero vane incidence, which is reasonable at design conditions, we consider a total-pressure loss coefficient, defined as $\omega = (P_{T,in} - P_{T,out})/(P_{T,in} - P_{in})$ equal to 0.25 for both components, and a pressure-recovery coefficient, i.e. $C_P = (P_{out} - P_{in})/(P_{T,in} - P_{in}) = 0.45$, for the return vane channel only [33]. At the exit of the second stage, a volute is prescribed as in the single-stage configuration. On the other hand, the extension to two-stage axial turbine is less complex and it does not require additional components to be modelled.

The optimized two-stage machine performance are reported in Figure 8 for selected conditions of pressure ratio and size parameter in terms of efficiency deviation $\Delta\eta$; this latter is defined as the difference between the two-stage optimized efficiency and the value provided by the correlations given in Eqs. (7) and (9) for single-stage compressors and turbines, respectively.

Upon examination of Figure 8(*a*), which reports the compressor-efficiency deviation, the application of two-stage compressors for $\beta_c < 3$ provides lower efficiency if compared to the corresponding single-stage configuration. Indeed, for these values of pressure ratio, a reduction in the aerodynamic loading and in its associated losses does not compensate the additional losses introduced by the crossover bend and the return vane channel. Otherwise, as long as the pressure ratio increases ($\beta_c > 3$),

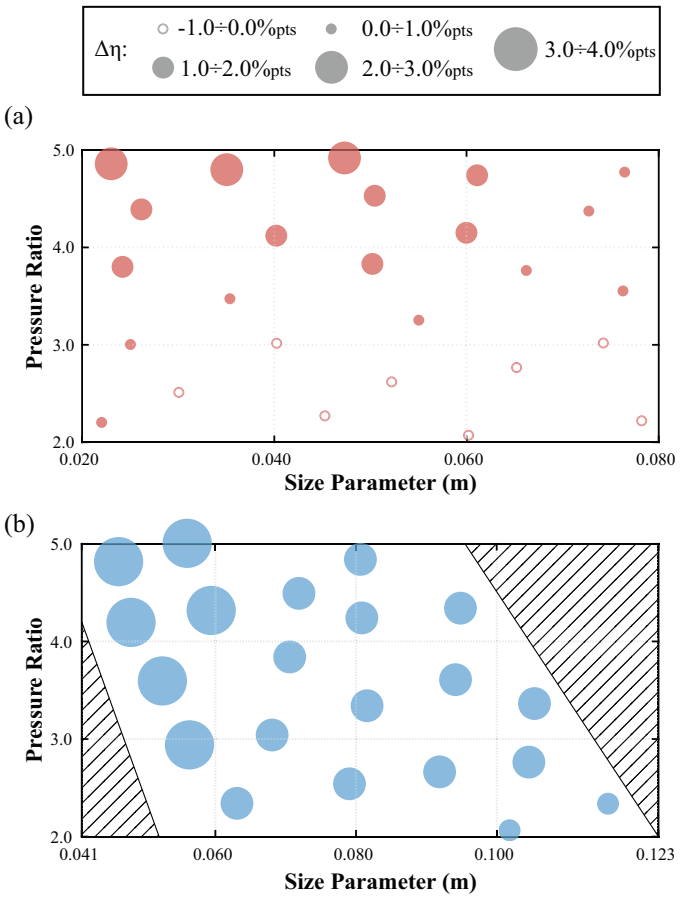

FIGURE 8: Efficiency deviation $\Delta\eta$ between dedicated optimizations of two-stage machines and predicted efficiencies by single-stage correlations for compressors (*a*) and turbines (*b*).

a positive efficiency gain is provided by the multi-stage solution, achieving up to $\Delta\eta_c = 2.0 \div 2.5$%pts at small size parameters ($SP_c < 0.05\,m$) and high pressure ratio ($\beta_c > 4.5$).

On the other hand, a two-stage turbine prevails over the single-stage layout for all the pressure ratio, as illustrated in Figure 8(*b*). Moreover, the efficiency gain provided by a multi-stage turbine is comparatively higher than the efficiency gain achievable by multi-stage compressors. Except for few designs located at high size parameters ($SP_t > 0.10\,m$) and low pressure ratio ($\beta_t < 2.5$), featuring an increase of about $\Delta\eta_t = 1.0 \div 1.5$%pts, the larger part of the mapped region exhibits a net increase of $\Delta\eta_t = 2 \div 3$%pts, which is extremely relevant as cycle performance are more affected by an increase in the turbine efficiency than in the compressor one [5]. Furthermore, for the lowest size-parameter values, i.e. $SP_t < 0.06\,m$, the efficiency gain raises to $\Delta\eta_t = 3 \div 4$%pts. For such optimized designs, the single-stage configuration converges to high values of rotational speed, close to the upper bound imposed in the optimization routine (see Table 4); the high peripheral speed required to obtain the work exchange combined with a limited angular speed results in a relatively large mean diameter, thus implying a comparably

This is a preprint of the following article: Romei, A., Gaetani, P., Giostri, A., & Persico, G., *The role of turbomachinery performance in the optimization of supercritical carbon dioxide power systems*, J. Turbomach., 2020.
The published article may differ from this preprint, and is available at the following DOI: 10.1115/1.4046182

small blade aspect ratio b/D_m. Relying on a multi-stage architecture, the aerodynamic loading on each stage is reduced, so that a smaller peripheral velocity is required. As a consequence, the optimization can find optimized machine designs which feature comparatively lower rotational speeds and higher blade aspect ratio, thus considerably reducing the weight of the secondary and, especially, of the leakage losses. A further increase in the number of stages, without additional constraints on the rotational speed, is expected to produce a significantly lower rise in the turbomachinery efficiency, as most of the losses, e.g. related to the blade loading and to the aspect ratio, are already minimized in the two-stage set up.

These optimized two-stage turbomachinery designs are used to formulate a correction for the correlations previously developed. To this end, a linear regression is used, exhibiting a coefficient of determination $R^2 = 0.75 \div 0.80$ for both the compressor $\Delta\overline{\eta}_c$ and the turbine $\Delta\overline{\eta}_t$ correction. The maximum deviation between the linear model prediction $\Delta\overline{\eta}$ and the actual deviation $\Delta\eta$ (as in Figure 8) is 0.75%pts and 0.50%pts for the compressor and the turbine, respectively, which are within the corresponding mean-line code errors. The analytical expressions for the linear corrections are:

$$\Delta\overline{\eta}_c = -0.15172\,SP_c + 0.00577\,\beta_c - 0.00671, \qquad (10)$$

$$\Delta\overline{\eta}_t = -0.20126\,SP_t + 0.00006\,\beta_t + 0.04447, \qquad (11)$$

where the subscript c refers to the compressor, whilst the subscript t refers to the turbine. These corrections have to be added to the single-stage machine correlations (refer to Eqs. (7) and (9) for compressor and turbine, respectively) to obtain the two-stage machine efficiency.

The corrected correlations are used to infer the potential cycle-efficiency gain brought by multi-stage turbomachinery, as illustrated in Figure 9. If a multi-stage solution performs worse than the corresponding single stage, i.e. $\Delta\overline{\eta} < 0$, this latter layout is considered for the selected cycle pressure ratio even in the multi-stage calculations. Two power-capacity targets are considered, namely $\dot{W}_{el} = 10\,\text{MW}$ and $\dot{W}_{el} = 50\,\text{MW}$ at fixed minimum and hot-source temperature, i.e. $T_{min} = 35\,^\circ\text{C}$ and $T_{max} = 750\,^\circ\text{C}$, respectively. Even at the smallest pressure ratio $\beta = 2$, the turbine-efficiency increase given by the multi-stage solution induces a substantial rise in the cycle efficiency, which results in $+0.6$%pts and $+1.0$%pts for high and low power capacity, respectively. As long as the pressure ratio increases, the marginal cycle improvement increases as well, achieving $+1.2$%pts and $+1.8$%pts at $\beta = 5$ for high and low power capacity, respectively. However, the expected efficiency gain given by a multi-stage turbomachinery arrangement must deal with the capital-cost increase, thus a trade-off between the increase of cycle performance and the plant cost has to be found. An optimum pressure ratio in the range $\beta = 2 \div 5$ also exists for multi-stage configurations, conversely to what predicted by the constant-efficiency assumption. Furthermore, significant quantitative differences between the efficiency predicted by the corrected correlations and the constant-efficiency assumption emerge, proving that this latter assumption is not suitable even when multi-stage arrangements are considered.

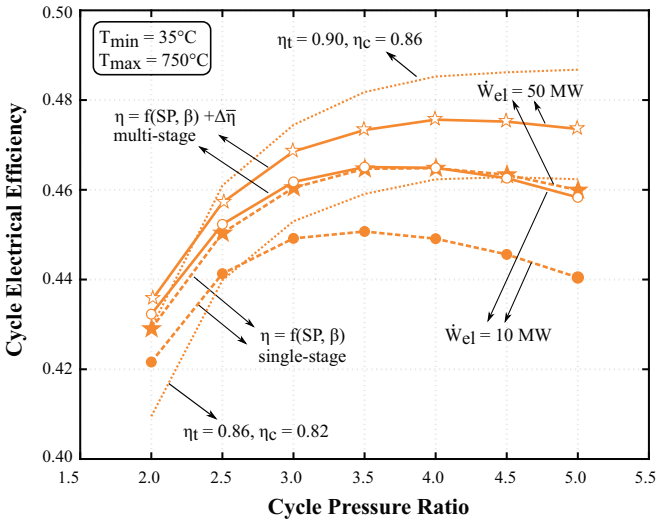

FIGURE 9: Cycle efficiency η_{el} evolution as a function of the cycle pressure ratio P_{max}/P_{min} for two installed power capacities by employing single- and multi-stage turbomachinery.

CONCLUSION

This work illustrates a detailed analysis about the impact of optimized turbomachinery performance on the efficiency of sCO_2 power cycles. The analysis is carried out numerically, combining a simulation tool for the design of recompression sCO_2 thermodynamic cycles with mean-line codes for both the compressor and the turbine, which are assumed to be of centrifugal and of axial architecture, respectively. The compressor mean-line tool is validated against experimental data along with a dedicated uncertainty-quantification analysis to include missing input information. The validation shows that nearly all data fall within the extended confidence intervals (± 1.5%pts for peak efficiencies at three different rotational speeds). The turbine mean-line code was validated in the past (± 2.0%pts against experiments) and used for several documented design tasks featuring real-gas effects. Turbomachinery designs are obtained by combining the mean-line codes with an external optimization routine implementing an evolutionary-based algorithm.

A comprehensive investigation about compressor maximum efficiency is performed by varying the intake-fluid thermodynamic conditions, the compressor pressure ratios and mass-flow rates. Three main conclusions are drawn from this analysis:

(I) Compressors optimized for conditions representative of full-scale plants exhibit competitive efficiencies ($82 \div 85$% for pressure ratio $\beta \leq 3.5$).

(II) The intake-fluid thermodynamic conditions seem not to affect the compressor efficiency if dedicated optimizations

This is a preprint of the following article: Romei, A., Gaetani, P., Giostri, A., & Persico, G., *The role of turbomachinery performance in the optimization of supercritical carbon dioxide power systems*, J. Turbomach., 2020.
The published article may differ from this preprint, and is available at the following DOI: 10.1115/1.4046182

are run ($\Delta\eta \leq 1.0\%$pts, within the uncertainty of the mean-line code).

(III) Appreciable differences in compressor efficiencies are found by changing the compressor size and loading. Compressor efficiencies reduces of $\approx 2\%$pts both by increasing the pressure-ratio value ($\Delta\beta = 1.5$) and by moving to lower mass-flow rates (e.g. from 250 kg/s to 50 kg/s).

Efficiency correlations accounting for size and aerodynamic loading effects are then deduced for single-stage compressors and turbines by fitting the optimized designs. These correlations are used to infer about thermodynamic cycle analyses and optimizations in a parametric way, changing the hot-source temperature, the minimum cycle temperature and the power capacity of the plant. The results are compared with those obtained by employing standard constant turbomachinery efficiencies. Qualitative (different trends of cycle electrical efficiency with respect to overall pressure ratio) and quantitative (cycle-efficiency differences up to $\approx 4\%$pts in the worst-case scenario) discrepancies suggest that a proper modelling of turbomachinery component is crucial to get reliable sCO_2 power-system optimizations.

Finally, a correction for multi-stage architectures is also devised, performing dedicated optimizations of two-stage turbomachinery. The corrected correlations are used to quantify the potential efficiency gain given by multi-stage turbomachinery arrangements, showing that small power-capacity plants are expected to benefit more from this choice (up to $+1.8\%$pts in terms of cycle efficiency). Furthermore, even for multi-stage configurations, constant turbomachinery-efficiency models are not able to properly reproduce the cycle-efficiency evolution, suggesting that a detailed turbomachinery model is still mandatory.

REFERENCES

[1] Dostal, V., 2004. "A supercritical carbon dioxide cycle for next generation nuclear reactors". PhD thesis, Massachusetts Institute of Technology.

[2] Neises, T., and Turchi, C., 2014. "A Comparison of Supercritical Carbon Dioxide Power Cycle Configurations with an Emphasis on CSP Applications". *Energy Procedia,* ***49***, pp. 1187 – 1196. Proceedings of the SolarPACES 2013 International Conference.

[3] Poerner, M., and Rimpel, A., 2017. "10 - Waste heat recovery". In *Fundamentals and Applications of Supercritical Carbon Dioxide (sCO) Based Power Cycles*, K. Brun, P. Friedman, and R. Dennis, eds. Woodhead Publishing, pp. 255 – 267.

[4] Musgrove, G., and Wright, S., 2017. "1 - Introduction and background". In *Fundamentals and Applications of Supercritical Carbon Dioxide (sCO_2) Based Power Cycles*, K. Brun, P. Friedman, and R. Dennis, eds. Woodhead Publishing, pp. 1 – 22.

[5] Allison, T., Moore, J., Pelton, R., Wilkes, J., and Ertas, B., 2017. "7 - Turbomachinery". In *Fundamentals and Applications of Supercritical Carbon Dioxide (sCO_2) Based Power Cycles*, K. Brun, P. Friedman, and R. Dennis, eds. Woodhead Publishing, pp. 147 – 215.

[6] Crespi, F., Gavagnin, G., Sánchez, D., and Martínez, G. S., 2017. "Analysis of the Thermodynamic Potential of Supercritical Carbon Dioxide Cycles: A Systematic Approach". *Journal of Engineering for Gas Turbines and Power,* ***140***(5), p. 051701.

[7] Wright, S. A., Radel, R. F., Vernon, M. E., Rochau, G. E., and Pickard, P. S., 2010. "Operation and analysis of a supercritical CO_2 Brayton cycle". *Sandia Report SAND2010-0171*.

[8] Noall, J. S., and Pasch, J. J., 2014. "Achievable Efficiency and Stability of Supercritical CO_2 Compression Systems Main Compressor Design Discussion". *The 4th International Symposium - Supercritical CO_2 Power Cycles September 2014*, pp. 1–10.

[9] Lemmon, E. W., Huber, M. L., and McLinden, M. O., 2013. "NIST reference database 23: reference fluid thermodynamic and transport properties–REFPROP, version 9.1". *Standard Reference Data Program*.

[10] Span, R., and Wagner, W., 1996. "A New Equation of State for Carbon Dioxide Covering the Fluid Region from the TriplePoint Temperature to 1100 K at Pressures up to 800 MPa". *Journal of Physical and Chemical Reference Data,* ***25***(6), pp. 1509–1596.

[11] Crespi, F., Gavagnin, G., Sanchez, D., and Martinez, G. S., 2017. "Supercritical carbon dioxide cycles for power generation: A review". *Applied Energy,* ***195***, pp. 152–183.

[12] Astolfi, M., Alfani, D., Lasala, S., and Macchi, E., 2018. "Comparison between ORC and CO_2 Power Systems for the exploitation of Low-Medium Temperature Heat Sources". *Energy,* ***161***, pp. 1250–1261.

[13] Oh, H. W., Yoon, E. S., and Chung, M. K., 1997. "An optimum set of loss models for performance prediction of centrifugal compressors". *Proceedings of the Institution of Mechanical Engineers, Part A: Journal of Power and Energy,* ***211***(4), pp. 331–338.

[14] Lee, J., Lee, J. I., Yoon, H. J., and Cha, J. E., 2014. "Supercritical Carbon Dioxide turbomachinery design for water-cooled Small Modular Reactor application". *Nuclear Engineering and Design,* ***270***, pp. 76–89.

[15] Ameli, A., Afzalifar, A., Turunen-Saaresti, T., and Backman, J., 2018. "Centrifugal compressor design for near-critical point applications". *Journal of Engineering for Gas Turbines and Power,* ***141***, pp. 1–8.

[16] Meroni, A., Zhlsdorf, B., Elmegaard, B., and Haglind, F., 2018. "Design of centrifugal compressors for heat pump systems". *Applied Energy,* ***232***, pp. 139–156.

[17] Wiesner, F. J., 1967. "A Review of Slip Factors for Centrifugal Impellers". *Journal of Engineering for Gas Turbines and Power,* ***89***(4), pp. 558–566.

[18] Aungier, R. H., 2000. *Centrifugal Compressors: A strategy for Aerodynamic Design and Analysis*. ASME PRESS.

[19] Jansen, W., 1967. "A method for calculating the flow in a centrifugal impeller when entropy gradients are present". In Royal Society Conference on Internal Aerodynamics (Turbomachinery), pp. 133–146.

[20] Lettieri, C., Baltadjiev, N. D., Casey, M., and Spakovszky, Z. S., 2014. "Low-Flow-Coefficient Centrifugal Compressor Design for Supercritical CO_2". *Journal of Turbomachinery,* ***136***(8), p. 081008.

[21] Wright, S. A., Pickard, P. S., Vernon, M. E., Radel, R. F., and Fuller, R., 2009. "Description and test results from a supercritical CO_2 Brayton cycle development program". *7th International Energy Conversion Engineering Conference*.

[22] Persico, G., and Pini, M., 2017. "8 - Fluid dynamic design of Organic Rankine Cycle turbines". In *Organic Rankine Cycle (ORC) Power Systems*, E. Macchi and M. Astolfi, eds. Woodhead Publishing, pp. 253 – 297.

[23] Wilson, D., 1984. *The Design of High–Efficiency Turbomachinery and Gas Turbines*. MIT Press.

[24] Craig, H. R. M., and Cox, H. J. A., 1970. "Performance estimation of axial flow turbines". *Proceedings of the Institution of Mechanical Engineers,* ***185***(1), pp. 407–424.

[25] Sawyer, J., 1972. *Gas Turbine Engineering Handbook*. Gas Turbine Publications, Stamford (CT).

[26] Zweifel, O., 1945. "The spacing of turbo-machine blading especially with large angular deection". *Brown Boveri Rev.,* ***32***, pp. 436–444.

[27] Casati, E., Vitale, S., Pini, M., Persico, G., and Colonna, P., 2014. Preliminary design method for small scale centrifugal ORC turbines. http://asme-orc2013.fyper.com/uploads/File/PPT%20155.pdf. Accessed: 10-26-2018.

[28] Bahamonde, S., Pini, M., De Servi, C., Rubino, A., and Colonna, P., 2017. "Method for the Preliminary Fluid Dynamic Design of High-Temperature Mini-Organic Rankine Cycle Turbines". *Journal of Engineering for Gas Turbines and Power,* ***139***(8).

[29] Pini, M., Persico, G., Casati, E., and Dossena, V., 2013. "Preliminary Design of a Centrifugal Turbine for Organic Rankine Cycle Applications". *Journal of Engineering for Gas Turbines and Power,* ***135***(4), p. 042312.

[30] Meroni, A., Andreasen, J. G., Persico, G., and Haglind, F., 2018. "Optimization of organic rankine cycle power systems considering multistage axial turbine design". *Applied Energy,* ***209***, pp. 339 – 354.
[31] Eckert, B., and Schnell, E., 1961. *Axial-und Radial- Kompressoren*. Springer Verlag.
[32] Whitfield, A., and Baines, N. C., 1990. *Design of radial turbomachines*. Longman Singapore Publishers (Pte) Ltd.
[33] Ludtke, K. H., 2004. *Process Centrifugal Compressors: Basics, Function, Operation, Design, Application*. Springer.
[34] Macchi, E., and Perdichizzi, A., 1981. "Efficiency Prediction for Axial-Flow Turbines Operating with Nonconventional Fluids". *Journal of Engineering for Power,* ***103***(4), p. 718.
[35] Macchi, E., and Astolfi, M., 2017. "9 - Axial flow turbines for Organic Rankine Cycle applications". In *Organic Rankine Cycle (ORC) Power Systems*, E. Macchi and M. Astolfi, eds. Woodhead Publishing, pp. 299 – 319.